Inorg. Chem. **2003**, *42*, 1256–1266

^{51}V Solid-State Magic Angle Spinning NMR Spectroscopy and DFT Studies of Oxovanadium(V) Complexes Mimicking the Active Site of Vanadium Haloperoxidases

Neela Pooransingh,[†] Ekaterina Pomerantseva,[†] Martin Ebel,[‡] Sven Jantzen,[‡] Dieter Rehder,*[,‡] and Tatyana Polenova*[,†]

Department of Chemistry, City University of New York—Hunter College, and the Graduate Center, 695 Park Avenue, New York, New York 10021, and Institut für Anorganische und Angewandte Chemie, Universität Hamburg, D-20146 Hamburg, Germany

Received October 29, 2002

A series of 11 oxovanadium(V) complexes mimicking the active site of vanadium haloperoxidases have been investigated by ^{51}V magic angle spinning NMR spectroscopy and density functional theory (DFT). The MAS spectra are dominated by the anisotropic quadrupolar and chemical shielding interactions; for these compounds, C_Q ranges from 3 to 8 MHz, and δ_σ is in the range 340–730 ppm. The quadrupolar coupling and chemical shielding tensors as well as their relative orientations have been determined by numerical simulations of the spectra. The spectroscopic NMR observables appear to be very sensitive to the details of the electronic and geometric environment of the vanadium center in these complexes. For the four crystallographically characterized compounds from the series, the quadrupolar and chemical shielding anisotropies were computed at the DFT level using two different basis sets, and the calculated tensors were in general agreement with the experimental solid-state NMR data. A combination of ^{51}V solid-state NMR and computational methods is thus beneficial for investigation of the electrostatic and geometric environment in diamagnetic vanadium systems with moderate quadrupolar anisotropies.

Introduction

Since the discovery of vanadium-containing enzymes two decades ago, there has been a growing interest in coordination chemistry of vanadium.[1] Vanadium complexes mimicking the active sites of vanadium haloperoxidases have attracted attention as putative oxidation and oxo transfer catalysts, and due to their potential medicinal applications.[2−5]

Vanadium haloperoxidases catalyze a two-electron oxidation of halide to hypohalous acid in the presence of hydrogen peroxide; the native enzymes require diamagnetic V(V) (vanadate covalently linked to a histidine) for their activity.[6−8] These enzymes, which are universally present in marine algae, and have also been found in fungi and lichens, are thought to be involved in the biosynthesis of halogenated natural products.[6,9] The kinetics and mechanism of haloperoxidases have been the subject of studies due to the potential utility of these enzymes in industrial-scale biocatalytic conversions: vanadium haloperoxidases are the most efficient halide oxidants known to date.[6] The recent X-ray crystal structures of vanadate-dependent chloro- and bromoperoxidases as well as the peroxide form of a chloroperoxidase highlighted the active site geometries, which were found to be strikingly similar.[10−12] Despite the wealth of experimental data about vanadium haloperoxidases, many

* To whom correspondence should be addressed. E-mail: tpolenov@hunter.cuny.edu (T.P.); rehder@chemie.uni-hamburg.de (D.R.). Phone: (212) 772-4310 (T.P.).

[†] City University of New York—Hunter College.

[‡] Universität Hamburg.

(1) Rehder, D. *Coord. Chem. Rev.* **1999**, *182*, 297−322.
(2) Colpas, G. J.; Hamstra, B. J.; Kampf, J. W.; Pecoraro, V. L. *Inorg. Chem.* **1994**, *33*, 4669−4675.
(3) Rehder, D.; Pessoa, J. C.; Geraldes, C. F. G. C. *JBIC, J. Biol. Inorg. Chem.* **2002**, *7*, 384−396.
(4) Thompson, K. H.; McNeill, J. H.; Orvig, C. *Chem. Rev.* **1999**, *99*, 2561−2571.
(5) Cornman, C. R.; Colpas, G. J.; Hoeschele, J. D.; Kampf, J.; Pecoraro, V. L. *J. Am. Chem. Soc.* **1992**, *114*, 9925−9933.
(6) Butler, A. *Coord. Chem. Rev.* **1999**, *187*, 17−35.
(7) Butler, A. *Curr. Opin. Chem. Bio.* **1998**, *2*, 279−285.
(8) Rehder, D. *BioMetals* **1992**, *5*, 3−12.
(9) Butler, A. *Science* **1998**, *281*, 207−210.
(10) Messerschmidt, A.; Prade, L.; Wever, R. *Biol. Chem.* **1997**, *378*, 309−315.
(11) Messerschmidt, A.; Wever, R. *Proc. Natl. Acad. Sci. U.S.A.* **1996**, *93*, 392−396.
(12) Weyand, M.; Hecht, H. J.; Kiess, M.; Liaud, M. F.; Vilter, H.; Schomburg, D. *J. Mol. Biol.* **1999**, *293*, 595−611.

10.1021/ic026141e CCC: $25.00
Published on Web 01/25/2003

aspects of their function and mechanism are unclear. The factors governing the substrate specificity, i.e., whether a particular enzyme will or will not display halogenating activity, are not understood, especially in light of the similar active site geometries of chloro- and bromoperoxidases.[13,14] A delicate balance of multiple interactions between the active site residues and the vanadium center, predominantly of medium strength electrostatic nature (hydrogen bonding), is currently thought to govern the specific halogenating activities of the haloperoxidases.[14] This hypothesis remains to be corroborated. It is of interest in this context that haloperoxidases have also been shown to exhibit sulfideperoxidase activity (enantioselective oxidation of prochiral sulfides to sulfoxides),[15,16] a potential which has been mimicked by oxovanadium(V) compounds which closely model the active center of the enzyme.[17,18]

In this work, we report a series of novel vanadium(V) complexes mimicking the active site of vanadium haloperoxidases. We have addressed these compounds by ^{51}V magic angle spinning spectroscopy as solid powders. We discuss the vanadium fine structure constants, namely the magnitudes and relative orientations of the quadrupolar and chemical-shielding anisotropy (CSA) tensors, in the context of coordination geometries and electronic properties of these model compounds. We demonstrate that the electrostatic environment of the vanadium atom(s) in these compounds is determined by the nature of both the proximal and the distal ligands and, thus, may differ significantly even when vanadium first coordination spheres are chemically and geometrically similar. For the four crystallographically characterized compounds of the series, we have computed the electric field gradient and chemical shielding anisotropy tensors with density functional theory. We found the results to be in general agreement with the experimental solid-state NMR data. The work reported herein demonstrates that a combination of ^{51}V solid-state NMR spectroscopy and theoretical calculations can be used as a sensitive quantitative probe of the local electronic environment of the transition metal.

Theoretical Considerations for ^{51}V Solid-State NMR Spectroscopy: Quadrupolar and Chemical Shielding Anisotropies

Solid-state NMR spectroscopy has been an important analytical tool for studies of inorganic materials and biological solids. During the past two decades, advances in hardware and experimental methodologies have resulted in expanding applications of solids NMR to complex inorganic and biological systems such as glasses, amorphous polymers, heterogeneous catalysts, and proteins. Multinuclear solid-state NMR experiments yield quantitative site-specific information for amorphous and crystalline solids, in bulk, on surfaces, and at the interfaces.[19] In particular, ^{51}V solid-state NMR spectroscopy is a rapidly emerging technique for analysis of vanadium-containing systems, including inorganic vanadates,[20−26] vanadium-based catalysts,[27−29] oxovanadium(V) alkoxides,[30] zeolites,[31] and metallorganic complexes.[32,33] ^{51}V is a half-integer quadrupolar nucleus ($I = {}^{7}/_{2}$) with high natural abundance (99.8%) and relatively high gyromagnetic ratio (Larmor frequency of 105.2 MHz at 9.4 T). The small quadrupolar moment allows direct observation of vanadium, and due to the favorable magnetic properties, small quantities of vanadium can be readily detected.

For half-integer spins, such as ^{51}V, the solid-state NMR spectra are dominated by a combination of the quadrupolar interaction (the interaction between the electric quadrupole moment of the nucleus and the electric field gradient on the nuclear site) and chemical-shielding anisotropy (CSA) (see refs 26 and 34 and references therein). The different magnitudes and different symmetry properties of the quadrupolar and chemical shielding anisotropies allow these tensorial quantities to be extracted from a single spectrum, along with the mutual orientations of the quadrupolar and CSA tensors.[26] The total Hamiltonian is

$$H = H_{\text{Zeeman}} + H_{\text{RF}} + H_{\text{DIP}} + H_{\text{Q}} + H_{\text{CSA}} \qquad (1)$$

The first three terms represent the Zeeman, the radiofrequency field, and the dipolar interactions. The last two terms are the quadrupolar and CSA interactions, which dictate the spectral shape. They are conveniently expressed in a spherical tensor notation in terms of the spatial (R_{mn})

(13) Butler, A.; Carter, J. N.; Simpson, M. T. *Vanadium in Proteins and Enzymes*; Bertini, I., Sigel, A., Sigel, H., Ed.; Marcel Dekker: New York, 2001; pp 153−179.
(14) Renirie, R.; Hemrika, W.; Wever, R. *J. Biol. Chem.* **2000**, *275*, 11650−11657.
(15) ten Brink, H. B.; Tuynman, A.; Dekker: H. L.; Hemrika, W.; Izumi, Y.; Oshiro, T.; Schoemaker, H. E.; Wever, R. *Inorg. Chem.* **1998**, *37*, 6780−6784.
(16) ten Brink, H. B.; Schoemaker, H. E.; Wever, R. *Eur. J. Biochem.* **2001**, *268*, 132−138.
(17) Rehder, D.; Santoni, G.; Licini, G. M.; Schulzke, C.; Meier, B. *Coord. Chem. Rev.*, in press.
(18) Bolm, C.; Bienewald, F. *Angew. Chem., Int. Ed. Engl.* **1996**, *34*, 2640−2642.
(19) Eckert, H. *Curr. Opin. Solid State Mater. Sci.* **1996**, *1*, 465−476.
(20) Gubanov, V. A.; Pletnev, R. N.; Lisson, V. N.; Chirkov, A. K. *Spectrosc. Lett.* **1977**, *10*, 527−532.
(21) Hayashi, S.; Hayamizu, K. *Bull. Chem. Soc. Jpn.* **1990**, *63*, 961−963.
(22) Nielsen, U. G.; Jacobsen, H. J.; Skibsted, J. *Inorg. Chem.* **2000**, *39*, 2135−2145.
(23) Nielsen, U. G.; Jacobsen, H. J.; Skibsted, J. *J. Phys. Chem. B* **2001**, *105*, 420−429.
(24) Skibsted, J.; Jacobsen, C. J. H.; Jacobsen, H. J. *Inorg. Chem.* **1998**, *37*, 3083−3092.
(25) Ganapathy, S.; Schramm, S.; Oldfield, E. *J. Chem. Phys.* **1982**, *77*, 4360−4365.
(26) Skibsted, J.; Nielsen, N. C.; Bildsøe, H.; Jacobsen, H. J. *Chem. Phys. Lett.* **1992**, *188*, 405−412.
(27) Miller, J. M.; Lakshmi, L. J. *J. Mol. Catal. A: Chem.* **1999**, *144*, 451−459.
(28) Shubin, A. A.; Lapina, O. B.; Bondareva, V. M. *Chem. Phys. Lett.* **1999**, *302*, 341−346.
(29) Lapina, O. B.; Mastikhin, V. M.; Shubin, A. A.; Krasilnikov, V. N.; Zamaraev, K. I. *Prog. Nucl. Magn. Reson. Spectrosc.* **1992**, *24*, 457−525.
(30) Crans, D. C.; Felty, R. A.; Chen, H.; Eckert, H.; Das, N. *Inorg. Chem.* **1994**, *33*, 2427−2438.
(31) Park, D. H.; Cheng, C. F.; Klinowski, J. *Bull. Korean Chem. Soc.* **1997**, *18*, 70−75.
(32) Rehder, D.; Paulsen, K.; Basler, W. *J. Magn. Reson.* **1983**, *53*, 500−502.
(33) Hampton, P. D.; Daitch, C. E.; Alam, T. M.; Pruss, E. A. *Inorg. Chem.* **1997**, *36*, 2879−2883.
(34) Smith, M. E.; van Eck, E. R. H. *Prog. Nucl. Magn. Reson. Spectrosc.* **1999**, *34*, 159−201.

and spin (T_{mn}) variables:[35]

$$H_Q^{(1)} = \frac{eQ}{4S(2S-1)} \cdot R_{20}^Q T_{20}^S = \omega_Q[3S_z^2 - S(S+1)] \quad (2)$$

$$H_Q^{(2)} = \frac{C_Q}{\omega_0} \sum_{m \neq 1} \frac{R_{2m} R_{2-m} [T_{2m}, T_{2-m}]}{2m} \quad (3)$$

$$H_{CSA} = -\gamma(R_{00}^{CS} T_{00}^S + R_{20}^{CS} T_{20}^S) = (\omega_{CS}^{iso} + \omega_{CS}^{aniso}) S_z \quad (4)$$

Upon spinning the solid powder sample at the magic angle (54.7°), the second-rank spatial components R_{20} of tensorial anisotropies of $H_Q^{(1)}$ and H_{CSA} are efficiently averaged into a spinning sideband pattern, while the fourth-rank terms of the $H_Q^{(2)}$ are preserved, resulting in a characteristic second-order lineshape of the individual spinning sidebands.

It has been demonstrated by Skibsted, Nielsen, Jacobsen, and their colleagues in a number of reports that the quadrupolar and the chemical-shielding anisotropy tensors, as well as their relative orientations, can be extracted with high precision by detecting the complete manifold of spinning sidebands from the central and the satellite transitions and subsequently simulating the spectra.[22−24,26,36−38] These tensorial interactions can be further correlated with the structure and electronic properties at the vanadium site. For compounds whose three-dimensional structures are not available, approximate estimates of the coordination geometries are obtained from the quadrupolar coupling constant and the asymmetry parameter of the EFG tensor, using a simple electrostatic model.[39] In the electrostatic model, the atoms in the first coordination sphere are treated as point charges, whose individual contributions to the electric field gradient on the central atom are combined to yield the net EFG tensor. This model is an oversimplification, which does not necessarily give precise quadrupolar interaction parameters, but it has been quite successful in predicting trends in homologous series of compounds.[22,23,39] In recent years, more rigorous quantum mechanical methods have been increasingly applied for calculations of the EFG tensors, which were experimentally found by solid-state NMR, Mössbauer spectroscopy, and other techniques.[40−46] In particular, density functional theory (DFT) has been increasingly used for computing the electric field gradients in solids, using both cluster[40,43,44] and extended periodic treatments.[40−42,45−47]

Experimental Section

Materials and Methods. The following compounds were prepared according to literature procedures: **VIII**,[48] **IX**,[49] **X**,[50] **XI**.[51] $VO(acac)_2$ [acac = acetylacetonate(1−)], 2-hydroxynaphthalene-1-carbaldehyde, 2-aminophenol, *o*-vanillin, benzoic acid hydrazide, maltol, kojic acid, 3-hydroxyflavone, benzhydroxamic acid, 2-aminomethylpyridine, and 3,5-bis(*tert*-butyl)catechol were obtained from commercial sources (Strem, Aldrich, Fluka). IR spectra were acquired on a Perkin-Elmer 1720 FT IR spectrophotometer in KBr pellets according to the standard procedures. Solution ^{1}H and ^{51}V NMR spectra were acquired on a Bruker AM 360 spectrometer. Isotropic chemical shifts are reported with respect to neat $VOCl_3$, whose ^{51}V spectrum was recorded and used as an external referencing standard. UV−vis spectra were acquired on a Varian 5E spectrophotometer in 1 cm cuvettes. EPR spectra were acquired on a Bruker 300E spectrometer at 9.47 GHz. Cyclic voltammetry was conducted with a Princeton Applied Research potentiostat 273A with the common 3-electrode arrangement (working electrode Pt foil, counter electrode Pt wire, calomel reference electrode); calibration was performed against Fc/Fc^+, 0.2 M TBAP was used as conducting salt, and scan rate was 100 mV s^{-1}.

Preparation of Ligands. *N*-(2-Hydroxyphenyl)-5,6-dibenzosalicylideneamine, L1a. 2-Hydroxynaphthalene-1-carbaldehyde (8.61 g (0.05 mol)) was dissolved in 100 mL of abs ethanol plus 100 mL of abs toluene and treated with 5.46 g (0.05 mol) of 2-aminophenol. The suspension was refluxed for 60 min, during which time orange to ochre solid azomethine separated. After cooling to room temperature, the solid was filtered off and washed with cold ethanol and hexane. After recrystallization from ethanol/hexane 3/1, the product was dried in vacuo. Yield 10.9 g (83%). Anal. Calcd for $C_{17}H_{13}NO_2$ (M = 263.32 g mol^{-1}): C, 77.55; H, 4.88; N, 5.32. Found: C, 77.27; H, 5.19; N, 5.56. IR (cm^{-1}): 3027 ν(C−H_{ar}); 1630 ν(C═N); 1599, 1585, 1514 ν(C═C); 1409 δ(O−H). ^{1}H NMR (DMSO-d_6): 6.75−8.39 (m, 10H, H_{ar}), 9.45 (s, 1H, CH═N).

***N*-(2-Hydroxyphenyl)-3-methoxy-salicylideneamine, L1b.** This ligand was prepared in analogy to **L1a** from 9.13 g (0.06 mol) of *o*-vanillin and 6.55 g (0.06 mol) of aminophenol in 100 mL of abs ethanol and 50 mL of abs toluene. The yield is 11.44 g (87%) of an intensively orange, microcrystalline solid. Anal. Calcd for $C_{14}H_{13}NO_3$ (M = 243.28 g mol^{-1}): C, 69.12; H, 5.39; N, 5.76. Found: C, 68.99; H, 5.39; N, 5.80. IR (cm^{-1}): 3040 ν(C−H_{ar}); 2829 ν(C−H_{OMe}); 1617 ν(C═N); 1602, 1509 ν(C═C); 1305 δ(O−H); 1246 ν(Ph−OMe). ^{1}H NMR (DMSO-d_6): 3.79 (s, 3H, OCH_3), 6.82−7.38 (m, 7H, H_{ar}), 8.95 (s, 1H, CH═N).

3-Methoxy-salicylidene-benzoylhydrazone, L2. To a solution of 4.08 g (0.03 mol) of benzoic acid hydrazide dissolved in 60 mL of ethanol was added over 10 min, under continuous stirring, a solution of 4.56 g (0.03 mol) of *o*-vanillin in 60 mL of ethanol.

(35) Frydman, L. *Annu. Rev. Phys. Chem.* **2001**, *52*, 463−498.
(36) Skibsted, J.; Nielsen, N. C.; Bildsøe, H.; Jacobsen, H. J. *J. Magn. Reson.* **1991**, *95*, 88−117.
(37) Skibsted, J.; Jakobsen, H. J. *Inorg. Chem.* **1999**, *38*, 1806−1813.
(38) Jacobsen, H. J.; Skibsted, J.; Bildsøe, H.; Nielsen, N. C. *J. Magn. Reson.* **1989**, *85*, 173−180.
(39) Koller, H.; Engelhardt, G.; Kentgens, A. P. M.; Sauer, J. *J. Phys. Chem.* **1994**, *98*, 1544−1551.
(40) Moore, E. A.; Johnson, C.; Mortimer, M.; Wigglesworth, C. *Phys. Chem. Chem. Phys.* **2000**, *2*, 1325−1331.
(41) Tsvyashchenko, A. V.; Fomicheva, L. N.; Magnitskaya, M. V.; Shirani, E. N.; Brudanin, V. B.; Filossofov, D. V.; Kochetov, O. I.; Lebedev, N. A.; Novgorodov, A. F.; Salamatin, A. V.; Korolev, N. A.; Velichkov, A. I.; Timkin, V. V.; Menushenkov, A. P.; Kuznetsov, A. V.; Shabanov, V. M.; Akselrod, Z. Z. *Solid State Commun.* **2001**, *119*, 153−158.
(42) Blaha, P.; Schwartz, K.; Herzig, P. *Phys. Rev. Lett.* **1985**, *54*, 1192−1195.
(43) Munro, O. Q.; Shabalala, S. C.; Brown, N. J. *Inorg. Chem.* **2001**, *40*, 3303−3317.
(44) Bryce, D. L.; Wasylishen, R. E. *Phys. Chem. Chem. Phys.* **2002**, *4*, 3591−3600.
(45) Bryant, P. L.; Harwell, C. R.; Wu, K.; Fronczek, F. R.; Hall, R. W.; Butler, L. G. *J. Phys. Chem. A* **1999**, *103*, 5246−5252.
(46) Marichal, C.; Kempf, J.-Y.; Maigret, B.; Hirschinger, J. *Solid State Nucl. Magn. Reson.* **1997**, *8*, 33−46.
(47) Schwarz, K.; Blaha, P. *Lect. Notes Chem* **1996**, *67*.
(48) Yamada, S.; Katayama, C.; Tanaka, J.; Tanaka, M. *Inorg. Chem.* **1984**, *23*, 253−255.
(49) Drew, R. E.; Einstein, F. W. B. *Inorg. Chem.* **1973**, *12*, 829−835.
(50) Wang, D. R.; Ebel, M.; Schulzke, C.; Gruning, C.; Hazari, S. K. S.; Rehder, D. *Eur. J. Inorg. Chem.* **2001**, *4*, 935−942.
(51) Maurya, M. R.; Khurana, S.; Zhang, W.; Rehder, D. *J. Chem. Soc., Dalton Trans.*, in press.

Table 1. Elemental Analyses, IR,[a] and Solution ^{1}H[b] and ^{51}V[c] Spectral Data

cmpd	empirical formula	M, g mol^{-1}	C (calcd) found	H (calcd) found	N (calcd) found	ν(C═N) cm^{-1}	ν(V═O) cm^{-1}	δ(^{51}V)	δ(^{1}H)
I SJZ0040	$C_{23}H_{16}NO_6V$	453.64	(60.94) 60.97	(3.56) 3.60	(3.09) 3.36	1622	968	−458	9.77
II SJZ0041	$C_{23}H_{16}NO_7V$	469.43	(58.86) 58.91	(3.44) 3.74	(2.98) 3.25	1618	968	−466	10.08
III SJZ0032	$C_{27}H_{21}N_2O_6V$	520.42	(62.32) 62.14	(4.07) 4.12	(5.38) 5.53	1601	971	−435	8.93[d]
IV SJZ0069	$C_{21}H_{17}N_2O_7V$	460.41	(54.80) 54.58	(3.72) 3.84	(6.09) 6.08	1607	982	−450	8.82
V SJZ0060	$C_{30}H_{21}N_2O_7V$	572.55	(62.95) 62.27	(3.70) 3.71	(4.89) 5.03	1605	972	−435[d]	9.00[d]
VI SJZ0068	$C_{28}H_{22}N_3O_6V$	547.54	(61.43) 60.97	(4.05) 4.00	(7.68) 7.66	1606	974	−436	9.08[e]
VII SJZ00108	$C_{29}H_{36}N_2O_{5.5}V$[f]	551.78	(62.25) 62.88	(6.48) 6.47	(5.01) 4.97	1626	945	+422, +375[g]	8.88
VIII HS001[j]								−523, −534[i]	
IX HS003[j]								−607[h]	
X Sal5OEt[j]								−399[d]	
XI VO_2(acpy-inh)[j]								−507	

[a] In KBr. [b] DMSO-d_6, if not indicated otherwise. [c] CD_2Cl_2, if not indicated otherwise. [d] $CDCl_3$. [e] Acetone-d_6. [f] The compound contains $^1/_2$ mol of ethanol of crystallization. [g] The ratio of the integral intensities is 1:1.7; the two signals possibly correspond to two isomers, cf. text. [h] In water. [i] In THF; the two signals are due to the presence of two diastereomeric pairs of enantiomers. [j] For **VIII**, **IX**, **X**, and **XI**, the chemical characterization data have been previously reported in refs 48, 49, 50, and 51, respectively. Herein, we report only the ^{51}V isotropic chemical shifts in solution.

The resulting suspension was refluxed for 45 min, cooled back to room temperature, and set to −30 °C for 2 h. The solid, which had precipitated, was filtered off, washed with ethanol, recrystallized from ethanol, and dried over P_4O_{10}. Yield 8.1 g (90%) of a cream solid. Analysis for $C_{15}H_{14}N_2O_3 \cdot H_2O$ (M = 288.3 g mol^{-1}): C, 62.49; H, 5.59; N, 9.72. Found: C, 62.47; H, 5.66; N, 9.60. IR (cm^{-1}): 3571 ν(H_2O); 3377, 3210 ν(N—H); 3062 ν(C—H_{ar}); 2839 ν(C—H_{OMe}); 1652 ν(CO); 1607 ν(C═N); 1576, 1497 ν(C═C); 1299 δ(O—H); 1247 ν(Ph—OMe). ^{1}H NMR (DMSO-d_6): 3.80 (s, 3H, OCH_3), 6.82−7.95 (m, 8H, H_{ar}), 8.65 (s, 1H, CH═N).

Preparation of Complexes. For all the oxovanadium complexes discussed in the following paragraphs, the elemental analyses, selected IR [ν(C═N), ν(V═O)], and solution NMR data [δ(^{51}V), δ(^{1}H) of the azomethine proton] are collated in Table 1.

Type VO(*ONO*)(*OO*) Complexes I−VI. The general procedure follows: $VO(acac)_2$ (0.06 g (2.26 mmol)) was dissolved in 40 mL of warm ethanol. To the green solution was added 2.26 mmol of the tridentate azomethine (*ONO*, **L1** or **L2**) ligand, which was stirred for 2 min, followed by the addition of 2.26 mmol of the bidentate (*OO*, **L3** or **L4**) ligand plus an additional 20 mL of ethanol. The reaction mixture was warmed to 50 °C and vigorously stirred for 60−90 min. The red-brown to red-black suspension thus obtained was cooled to room temperature. The solid was filtered off, washed with several portions of ethanol and hexane, and dried in vacuo.

Maltolato-{*N*-(2-oxiphenyl)-5,6-dibenzosalicylideneaminato}-oxovanadium(V), [VO(L1a)L3a], I. Yield 0.85 g (83%); dark brown solid. IR (cm^{-1}): 3057 ν(C—H_{ar}); 1596 ν(C═O); 1201 ν(C—O_{maltol}). ^{1}H NMR ($CDCl_2$): 2.65 (s, 3H, CH_3), 6.63−8.33 (m, 10H, H_{ar}), 6.41 and 7.88 (d, 1H each, H_{maltol}).

Kojiccarboxylato-{*N*-(2-oxiphenyl)-5,6-dibenzosalicylideneaminato}-oxovanadium(V), [VO(L1a)L3c], II. Yield 0.8 g (75%); brown solid. IR (cm^{-1}): 3300 ν(O—H); 3080 ν(C—H_{ar}); 2925 ν(C—H_2); 1626 ν(C═C); 1597 ν(C═O); 1223 ν(C—O_{kojic}). ^{1}H NMR ($CDCl_2$): 4.41 (s, 2H, CH_2), 6.85−8.68 (m, 10H, H_{ar}), 6.57 and 8.51 (d, 1H each, H_{kojic}).

Benzhydroxamato-{*N*-(2-oxiphenyl)-5,6-dibenzosalicylideneaminato}-oxovanadium(V), [VO(L1b)L4], III. Yield 0.85 g (72%); brown solid. IR (cm^{-1}): 3065 ν(C—H_{ar}); 2839 ν(C—H_{OMe}); 1257 ν(Ph—OMe). ^{1}H NMR ($CDCl_3$): 3.93 (s, 3H, OCH_3), 6.78−7.42 (m, 7H, H_{ar}). $E_{1/2}$ (MeCN, vs SCE) −10 mV.

Maltolato-{3-methoxisalicylidene-α-(oxibenzylidenehydrazonato)}-oxovanadium(V), [VO(L2)L3a], IV. Yield 0.9 g (87%); black solid. IR (cm^{-1}): 3058 ν(C—H_{ar}); 2963, 2936 ν(C—H_{Me}); 2839 ν(C—H_{OMe}); 1620 ν(C═C); 1259 ν(Ph—OMe). ^{1}H NMR (CD_2Cl_2): 2.68 (s, 3H, OCH_3), 6.42 and 7.88 (d, 1H each, H_{maltol}), 6.96−7.98 (m, 18H, H_{ar}). $E_{1/2}$ (MeCN, vs SCE): −12 mV.

3-Oxiflavone-{3-Methoxisalicylidene-α-(oxibenzylidenehydrazonato)}-oxovanadium(V), [VO(L2)L3b], V. Yield 1.91 g (92%); deep brown solid. IR (cm^{-1}): 3062 ν(C—H_{ar}); 2840 ν(C—H_{OMe}); 1539 ν(C═O); 1261 ν(Ph—OMe); 1208 ν(C—$O_{flavone}$). ^{1}H NMR ($CDCl_3$): 3.81 (s, 3H, OCH_3), 7.99 and 8.60 (d, 1H each, $H_{flavone}$), 6.98−8.12 (m, 8H, H_{ar}).

Benzhydroxamato-(3-methoxi-α-hydroxybenzylidenehydrazonato)-oxovanadium(V), [VO(L2)L4], VI. Yield 0.75 g (61%); dark red-brown solid. IR (cm^{-1}): 3063 ν(C—H_{ar}); 2834 ν(C—H_{OMe}); 1559 ν(C═O); 1259 ν(Ph—OMe). ^{1}H NMR ($CDCl_3$): 3.91 (s, 3H, OCH_3), 6.99−8.07 (m, 8H, H_{ar}).

VO(*ONN*)(*OO*), VII. Acetylacetonato-{*N*-(2-methylpyridine)-3-methoxy-salicylideneaminato}-oxovanadium(IV), [VO(acac)-ONN]. To a solution of 3.83 g (35.4 mmol) of 2-aminomethylpyridine in 80 mL of ethanol was added dropwise 50 mL of an ethanolic solution of 5.38 g (35.4 mmol) of *o*-vanillin. The golden-yellow solution was refluxed for 60 min and cooled back to room temperature, upon which the solution turned orange. After removal of oxygen and saturation of the solution with N_2, 60 mL of an ethanolic solution containing 9.38 g (35.4 mmol) of $VO(acac)_2$ was added under nitrogen and the mixture refluxed for 45 min. The solution was cooled to room temperature and the solid filtered off and washed with ethanol until the filtrate was colorless. The solid residue was finally washed with several portions of pentane and dried in vacuo. Yield 10.47 g (73%) of black-green VO(acac)*ONN*. Anal. Calcd for $C_{19}H_{20}N_2O_5V$ (M = 407.45 g mol^{-1}): C, 56.03; H, 4.95; N, 6.88. Found: C, 55.95; H, 4.99; N, 6.87. IR (cm^{-1}): 3061, 3003 ν(C—H_{ar}); 2962, 2924 ν(C—H_{aliph}); 2837 ν(C—H_{OMe}); 1631 ν(C═N); 1601 ν(C═O); 1516 ν(C═C_{acac}); 1248 ν(Ph—OMe); 950 ν(V═O). EPR (CH_2Cl_2, 100 K): g_z = 1.950, A_z 177.1 × 10^{-4} cm^{-1}; g_{xy} 1.979, A_{xy} 65.2 × 10^{-4} cm^{-1}. UV−vis (DMSO, λ_{max} [nm], (ϵ [cm mmol^{-1}])): 287 (20070), 341 (4360), 399 (3640). $E_{1/2}$ (MeCN, vs SCE): 550 mV.

(3,5-Di-^{t}Bu-catecholato)-{*N*-(2-methylpyridine)-3-methoxy-salicylideneaminato}-oxovanadium(V), [VO(L5)L6], VII. VO(acac)*ONN* (1.6 mmol) was suspended in 60 mL of ethanol and treated, with vigorous stirring, with 0.36 g (1.6 mmol) of 3,5-bis(*tert*-butyl)catechol and an additional 20 mL of ethanol. The color changed from blue to blue-violet. The reaction mixture was stirred on a water bath for 60 min, cooled to room temperature, and stirred overnight. The solution was finally concentrated to about half of its volume and treated with ca. 15 mL of pentane and the solid precipitate filtered off, washed with pentane, and dried under vacuum. Yield 0.65 g (75%); violet solid. IR (cm^{-1}): 3058 ν(C—H_{ar}); 2953, 2905, 2867 ν(C—H_{aliph}); 2834 ν(C—H_{OMe}); 1601, 1580 ν(C═C_{ar}); 1248 ν(Ph—OMe). ^{1}H NMR (DMSO-d_6): 1.17 and 1.23

(s, 9H each, CMe_3), 3.70 (s, 3H, OCH_3), 5.55 (dd, 2H, CH_2), 6.70−8.18 (m, 9H, H_{ar}). UV−vis (DMSO, λ_{max} [nm], (ϵ [cm mmol^{-1}])): 289 (4310), 548 (1485), 860 (1585).

MAS NMR Spectroscopy. ^{51}V solid-state NMR spectra were acquired at 105.2 MHz (9.4 T) on a Tecmag Discovery spectrometer using a 4 mm Doty XC4 MAS probe. Spectra were recorded using 5−40 mg of sample. For each of the compounds, spectra at three different spinning speeds ranging between 10 and 17 kHz were acquired. The spinning speed was controlled to within ±5 Hz. The magic angle was adjusted using $NaNO_3$ (by detecting the ^{23}Na MAS signal), which is accurate to ±0.005°. A single 1 μs pulse ($\gamma H_1/2\pi \approx 80$ kHz) was employed to excite the central and the satellite transitions; 0.5 s recycle delays were used. The spectral widths were 1.25 MHz. 4096 complex data points were acquired. The data were processed by linear prediction of the first 66 points to suppress baseline distortions, followed by Fourier transformation and baseline correction using the MestRe-C23 NMR data processing software.[52] Isotropic chemical shifts are reported with respect to neat $VOCl_3$, whose ^{51}V spectrum was recorded and used as an external referencing standard.

Simulations of the NMR Spectra. Numerical simulations of the experimental ^{51}V solid-state NMR spectra were performed on a 1.1 GHz Pentium-4 PC under the Linux environment using the SIMPSON software package.[53] The combined effect of the quadrupolar interaction to second-order and chemical-shielding anisotropy was taken into account in the simulations. The seven independent parameters describing the quadrupolar and CSA tensor anisotropies (C_Q, η_Q, δ_σ, and η_σ) and the relative tensor orientations (the Euler angles α, β, and γ) were obtained by the least-squares fitting of the simulated and experimental sideband intensities using a program written in our laboratory under the Mathematica (Wolfram, Inc.) environment. The quality factor of the probe (Q) has been taken into account in the simulations. The quadrupolar and CSA tensor elements are defined in a spherical harmonics basis set according to the standard notation:[54]

$$C_Q = \frac{eQV_{zz}}{h} \quad \eta_Q = \frac{V_{yy} - V_{xx}}{V_{zz}}$$

$$\delta_\sigma = \delta_{iso} - \delta_{33} \quad \eta_\sigma = \frac{\delta_{22} - \delta_{11}}{\delta_{33}} \quad \delta_{iso} = {}^1/_3(\delta_{11} + \delta_{22} + \delta_{33}) \quad (5)$$

where C_Q is the quadrupolar coupling constant (in MHz); V_{xx}, V_{yy}, V_{zz} are the principal components of the electric field gradient (EFG) tensor, with $V_{zz} = eq$ being its largest principal component; Q is the vanadium quadrupole moment (-0.052×10^{-28} V/m^2);[34] e is the electronic charge; h is the Planck constant. δ_{iso} is the isotropic chemical shift; δ_{11}, δ_{22}, and δ_{33} are the principal components of the CSA tensor, with $\delta_{11} \le \delta_{22} \le \delta_{33}$ (δ_{33} is the most shielded component). η_Q and η_σ are the asymmetry parameters of the EFG and CSA tensors, respectively.

Calculation of Quadrupolar Interaction Parameters. Quadrupolar coupling constant, C_Q, and the asymmetry parameter of the EFG tensor, η_Q, were calculated using the classical electrostatic model,[24,39] as well as quantum mechanically, using density functional theory implemented in Gaussian98.[55] For the electrostatic point monopole calculations, charges on the atoms in the first coordination sphere of the ^{51}V nucleus were estimated from empirical relationships using the bond-valence approach.[56,57] On the basis of the crystallographic coordinates and charges of each atom in the first coordination sphere, the matrix giving the electric field gradient at the central vanadium nucleus was calculated, with the nine entries $V_{ij} = ne(3_{ij}/r^5 - \delta_{ij}/r^3)$, where e is the electronic charge, ne is the charge on each atom, i and j are the Cartesian x, y, or z coordinates of the ligand atom (assuming the coordinates of the central vanadium are (0, 0, 0)), and r is the distance between the ligand and the central vanadium atom. The matrices representing the individual contributions from each of the ligand atoms were subsequently summed, and the resulting tensor was diagonalized to obtain its principal components. The largest principal value V_{zz}=eq was used to calculate the quadrupolar coupling constant $C_Q = (1 - \gamma_\infty)\cdot(e^2qQ/h)$, where γ_∞ is the Sternheimer antishielding factor[58] (−7.6 for ^{51}V).[34] The asymmetry parameter of the electric field gradient was calculated from the principal components of the EFG tensor using the definition in the previous section. Preliminary calculations were performed using a PC program written in Pascal (courtesy of Dr. Arno P. M. Kentgens, University of Nijmegen, The Netherlands), and the calculations reported in this work employed a PC program written in our laboratory under the Mathematica environment. The program is available at http://patsy.hunter.cuny.edu/FandS/TP/MATHEMATICA/Quadrupolar_tensor_calculation.nb.

The DFT calculations of electric field gradient and nuclear magnetic shielding tensors were performed under Gaussian98;[55] Becke's three-parameter hybrid B3LYP functional was used.[59] The TZV basis set[60] and effective core potentials for vanadium atoms were used for one set of the calculations; in another set of calculations, the 6-311+G basis set was employed. The nuclear magnetic shielding calculations were performed using the gauge-including atomic orbitals (GIAO) method,[61,62] as implemented in Gaussian98. The calculated isotropic chemical shieldings are reported with respect to $VOCl_3$ optimized at the same level of theory. The computed absolute shieldings for $VOCl_3$ were −2415.2 ppm and −2374.4 ppm for the TZV and 6-311+G basis sets, respectively.

Results and Discussion

Synthesis and Characterization of the VO(*ONO*)(*OO*) Type Complexes. The complexes were prepared by addition

(52) Cobas, J.; Cruces, J.; Sardina, F. J. *MestRe-C: Magnetic Resonance Companion*; Departamento de Quimica Organica, Facultat de Quimica. Universidad de Santiago de Compostela: Spain, 2000.
(53) Bak, M.; Rasmussen, J. T.; Nielsen, N. C. *J. Magn. Reson.* **2000**, *147*, 296−330.
(54) Schmidt-Rohr, K.; Spiess, H. W. *Multidimensional Solid-State NMR and Polymers*; Hartcourt Brace & Company: London, 1999.
(55) Frisch, M. J.; Trucks, G. W.; Schlegel, H. B.; Scuseria, G. E.; Robb, M. A.; Cheeseman, J. R.; Zakrzewski, V. G.; Montgomery, J. A., Jr.; Stratmann, R. E.; Burant, J. C.; Dapprich, S.; Millam, J. M.; Daniels, A. D.; Kudin, K. N.; Strain, M. C.; Farkas, O.; Tomasi, J.; Barone, V.; Cossi, M.; Cammi, R.; Mennucci, B.; Pomelli, C.; Adamo, C.; Clifford, S.; Ochterski, J.; Petersson, G. A.; Ayala, P. Y.; Cui, Q.; Morokuma, K.; Malick, D. K.; Rabuck, A. D.; Raghavachari, K.; Foresman, J. B.; Cioslowski, J.; Ortiz, J. V.; Stefanov, B. B.; Liu, G.; Liashenko, A.; Piskorz, P.; Komaromi, I.; Gomperts, R.; Martin, R. L.; Fox, D. J.; Keith, T.; Al-Laham, M. A.; Peng, C. Y.; Nanayakkara, A.; Gonzalez, C.; Challacombe, M.; Gill, P. M. W.; Johnson, B. G.; Chen, W.; Wong, M. W.; Andres, J. L.; Head-Gordon, M.; Replogle, E. S.; Pople, J. A. *Gaussian 98*, revision A.1x; Gaussian, Inc.: Pittsburgh, PA, 1998.
(56) Brown, I. D.; Shannon, R. D. *Acta Crystallogr.* **1973**, *A29*, 266−282.
(57) Brown, I. D.; Altermatt, D. *Acta Crystallogr.* **1985**, *B41*, 244−247.
(58) Beri, A. C.; Lee, T.; Das, T. P.; Sternheimer, R. M. *Phys. Rev. B* **1983**, *28*, 2335−2351.
(59) Becke, A. D. *J. Chem. Phys.* **1993**, *98*, 5648−5652.
(60) Schafer, A.; Huber, C.; Ahlrichs, R. *J. Chem. Phys.* **1994**, *100*, 5829−5835.
(61) Ditchfield, R. *Mol. Phys.* **1974**, *27*, 789−807.
(62) Wolinski, K.; Hinton, J. F.; Pulay, P. *J. Am. Chem. Soc.* **1990**, *112*, 8251−8260.

Scheme 1

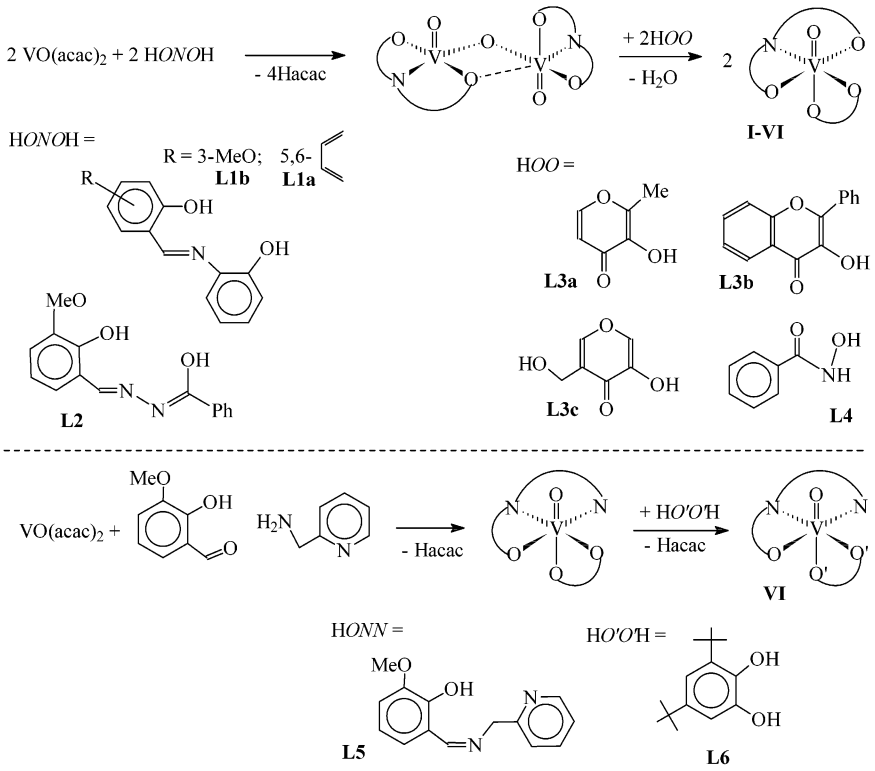

of the azomethine ligand (H_2ONO, Schiff base ligands **L1** or hydrazones **L2**) to $VO(acac)_2$ in ethanolic solution under aerobic conditions, followed by addition of the bidentate ligand (H*OO*, maltol derivatives **L3** or bezohydroxamic acid **L4**) in a one-pot reaction according to Scheme 1. In a first step, the two acetylacetonato ligands of the precursor compound are replaced by the azomethine, and V^{IV} is oxidized to V^{V}. These intermediates can be isolated and identified by their spectral characteristics; similar complexes have been described previously.[63,64] In a second step, the intermediately formed dinuclear, oxo-bridged complex reacts with the bidentate ligand to form the mononuclear target compounds **I**−**VI**. Where the azomethine ligand is a hydrazone, it reacts out of its enol form (**L2** in Scheme 1), documented by the lack of a C═O stretch in the IR. To obtain defined products, it appears to be essential that, in the bidentate ligand, (i) the OH is sufficiently acidic (i.e., bound to an sp^2 hybridized C, or to N), and (ii) a five-membered chelate ring forms. The isolation of the complexes is facilitated by their stability in air and their low solubility in ethanol. They have been obtained in yields around 85%. Identification was carried out by elemental analysis and IR and solution NMR spectroscopies (Table 1).

All of the compounds show the characteristic ν(V═O) between 968 and 982 cm^{-1}. The ν(C═O) of the bidentate ligands **L3** and **L4** is shifted to lower wavenumbers in the complexes by 60−70 cm^{-1}, pointing toward an axial orientation (*trans* to the doubly bonded oxo group) of the carbonyl oxygen. A *cis* (equatorial) orientation as in acetylacetonato complexes of vanadium gives rise to a low-frequency shift of about 100 cm^{-1}. Consequently, the tridentate ligand occupies meridional positions in the overall octahedral structure, as indicated schematically in Scheme 1. The axial + equatorial orientation of the OO ligand is corroborated by structure evidence for related maltolato[65] and hydroxamato[66] complexes. A shift of only several wavenumbers to lower values is noted for the ν(C═N). The solution ^{51}V NMR spectra in DMSO-d_6 show a single resonance in the −435 to −465 ppm region expected for complexes containing an O_5N donor set.[67] Because the steric conditions in the complexes are about the same, differences in the shielding should be due to differentiation in the electronic situation. ^{1}H NMR characteristics are in accord with the proposed formulations of the complexes. The proton of the azomethine group in the complexed ligand, between δ = 8.8 and 10.1, is shifted to higher magnetic field with respect to the uncoordinated, protonated ligand by 0.2−0.5 ppm.

Synthesis and Characterization of VO(*ONN*)(cat). Catecholatovanadium complexes are of importance in the context of the reduction of vanadate, storage of VO^{2+} and V^{III}, and tunichrome synthesis with vanadium templates by certain branches of sea squirts (*Ascidiaceae*).[68] VO(*ONN*)(cat) (cf. **VII** in Scheme 1) was obtained in a two step reaction. The

(63) Dutta, S.; Basu, P.; Chakravorty, A. *Inorg. Chem.* **1993**, *32*, 5343−5348.
(64) Schmidt, H.; Bashirpoor, M.; Rehder, D. *J. Chem. Soc., Dalton Trans.* **1996**, *19*, 3865−3870.
(65) Caravan, P.; Gelmini, L.; Glover, N.; Herring, F. G.; Li, H. L.; McNeill, J. H.; Rettig, S. J.; Setyawati, I. A.; Shuter, E.; Sun, Y.; Tracey, A. S.; Yuen, V. G.; Orvig, C. *J. Am. Chem. Soc.* **1995**, *117*, 12759−12770.
(66) Gao, S.; Weng, Z. Q.; Liu, S. X. *Polyhedron* **1998**, *17*, 3595−3606.
(67) Rehder, D.; Weidemann, C.; Duch, A.; Priebsch, W. *Inorg. Chem.* **1988**, *27*, 584−587.

Table 2. Plausible Structures of the Oxovanadium(V) Complexes[a]

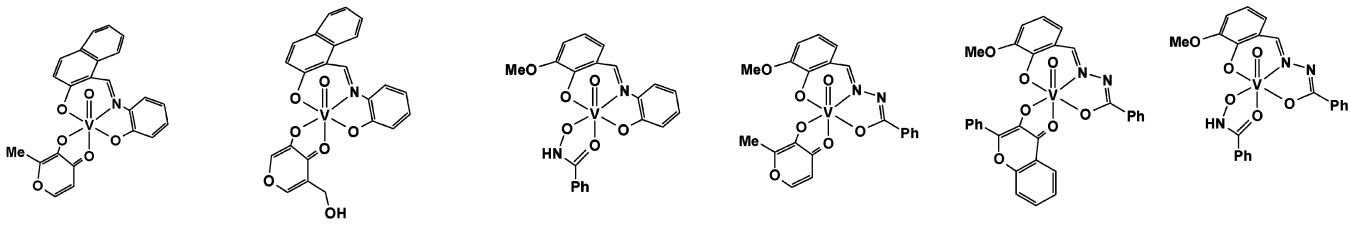

SJZ0040 **(I)** SJZ0041 **(II)** SJZ0032 **(III)** SJZ0069 **(IV)** SJZ0060 **(V)** SJZ0068 **(VI)**

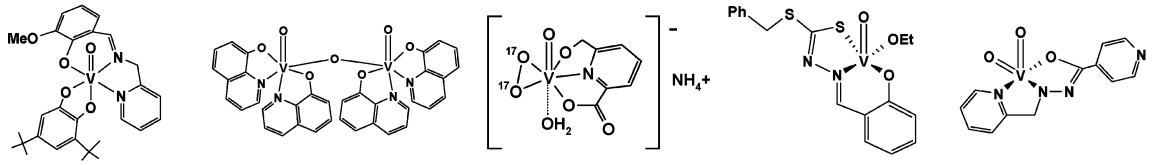

SJZ00108 **(VII)** HS001* **(VIII)** HS003* **(IX)** Sal50Et* **(X)** VO_2[acpy-inh]* **(XI)**

[a] Asterisk indicates that, for these compounds, the X-ray crystal structures have been reported: **VIII**,[48] **IX**,[49] **X**,[50] and **XI**[73].

first step is the formation of VO(*ONN*)(acac) by reacting $VO(acac)_2$ with *o*-vanillin and 2-aminomethylpyridine. The vanadyl ion acts as a template for the formation of the *ONN* Schiff base **L5**. VO(*ONN*)(acac) has been isolated and characterized, cf. Experimental Section. The second step is the replacement of the second acetylacetonate by 3,5-di(*tert*-butyl)catechol (**L6**) in ethanol with concomitant aerial oxidation of V^{IV} to V^{V} to yield complex **VII**. Alternatively, the complex can be generated from $VO(O^iPr)_3$, the Schiff base **L5**, and the catechol **L6** in abs THF. The proposed structure of **VII**, with the catecholate in the axial/equatorial position, is based on those of structurally characterized, related catecholato complexes.[5,69] This formulation is in accord with characteristic spectroscopic data [ν(V=O) 945, ν(CH=N) 1626; $\delta(^1H)_{CH=N}$ 8.88]. A remarkable feature of this and other complexes containing the "noninnocent" catecholato ligand[5,69,70] is the substantial deshielding of the ^{51}V nucleus, giving rise to chemical shifts $\delta(^{51}V) = +422$ and $+375$ ppm. The presence of two signals in DMSO solution may hint toward two isomers present in solution, generated by axial coordination of the phenolate oxo group in position 1 and 2, respectively, of the catecholate. The deshielding goes along with strong LMCT bands at 548 and 860 nm ($\epsilon = 1490$ and 1590 $cm^2\ mmol^{-1}$).

Anisotropic Lineshapes and Isotropic Chemical Shifts in the ^{51}V Solid-State MAS Spectra of Vanadium(V) Complexes. In Table 2, the plausible structures of the *ONO*-vanadium(V) compounds under investigation are summarized. In Figure 1, the experimental ^{51}V magic angle spinning spectra acquired at 15 kHz for each of the compounds are presented. Strongly asymmetric lineshapes in all of the compounds indicate large chemical shielding anisotropies. The spectra appear to be very sensitive to the details of the chemical environment at the vanadium site, displaying a broad repertoire of asymmetric anisotropic lineshapes. Qualitatively, this is reflected in the overall breadth of the spectral envelope (which is dictated by the strength of the quadrupolar coupling, C_Q), in the overall shape of the spectral envelope (dictated by the asymmetry of the quadrupolar tensor, η_Q), in the degree of the asymmetry, and in the overall shape of the sidebands corresponding to the central transition (dictated by the magnitude and the asymmetry of the CSA tensor, δ_σ and η_σ, respectively). It is not only the nature of the proximal ligands but also the nature of the distal substituents that appear to be an important determinant of the spectral lineshape, as can be inferred from comparison of the MAS spectra for **I**−**VI**. This series contains compounds with identical proximal ligands and different distal substituents; the NMR spectral lineshapes differ for each of the compounds.

The isotropic chemical shifts are compiled in Table 3. The second-order quadrupole induced shifts were taken into account as a correction to the experimentally observed isotropic sideband according to the following:[71]

$$\delta_{obsd} - \delta_{iso} = \frac{-3 \times 10^{-6}(e^2qQ/h)^2[I(I+1) - 9m(m-1) - 3][1 + {}^{\eta^2}/_3]}{40({\nu_0}^2)[I(2I-1)]^2} \quad (6)$$

where (e^2qQ/h) is the quadrupolar coupling constant (C_Q, in MHz), I is the spin number, $I = {}^7/_2$ for ^{51}V, m is the magnetic spin number ($m = {}^1/_2$ for the central transition), η is the asymmetry of the CSA tensor, and ν_0 is the resonance frequency of the ^{51}V nucleus (105.2 MHz at 9.4 T).

The second-order quadrupole-induced shifts cause substantial discrepancies between the experimentally observed isotropic sidebands and the genuine isotropic chemical shift

(68) Smith, M. J.; Kim, D.; Horenstein, B.; Nakanishi, K.; Kustin, K. *Acc. Chem. Res.* **1991**, *24*, 117−124.
(69) Cornman, C. R.; Kampf, J.; Pecoraro, V. L. *Inorg. Chem.* **1992**, *31*, 1981−1983.
(70) Kabanos, T. A.; Slawin, A. M. Z.; Williams, D. J.; Woollins, J. D. *J. Chem. Soc., Chem. Commun.* **1990**, *2*, 193−194.
(71) Kundla, E.; Samoson, A.; Lipmaa, E. *Chem. Phys. Lett.* **1981**, *83*, 229.

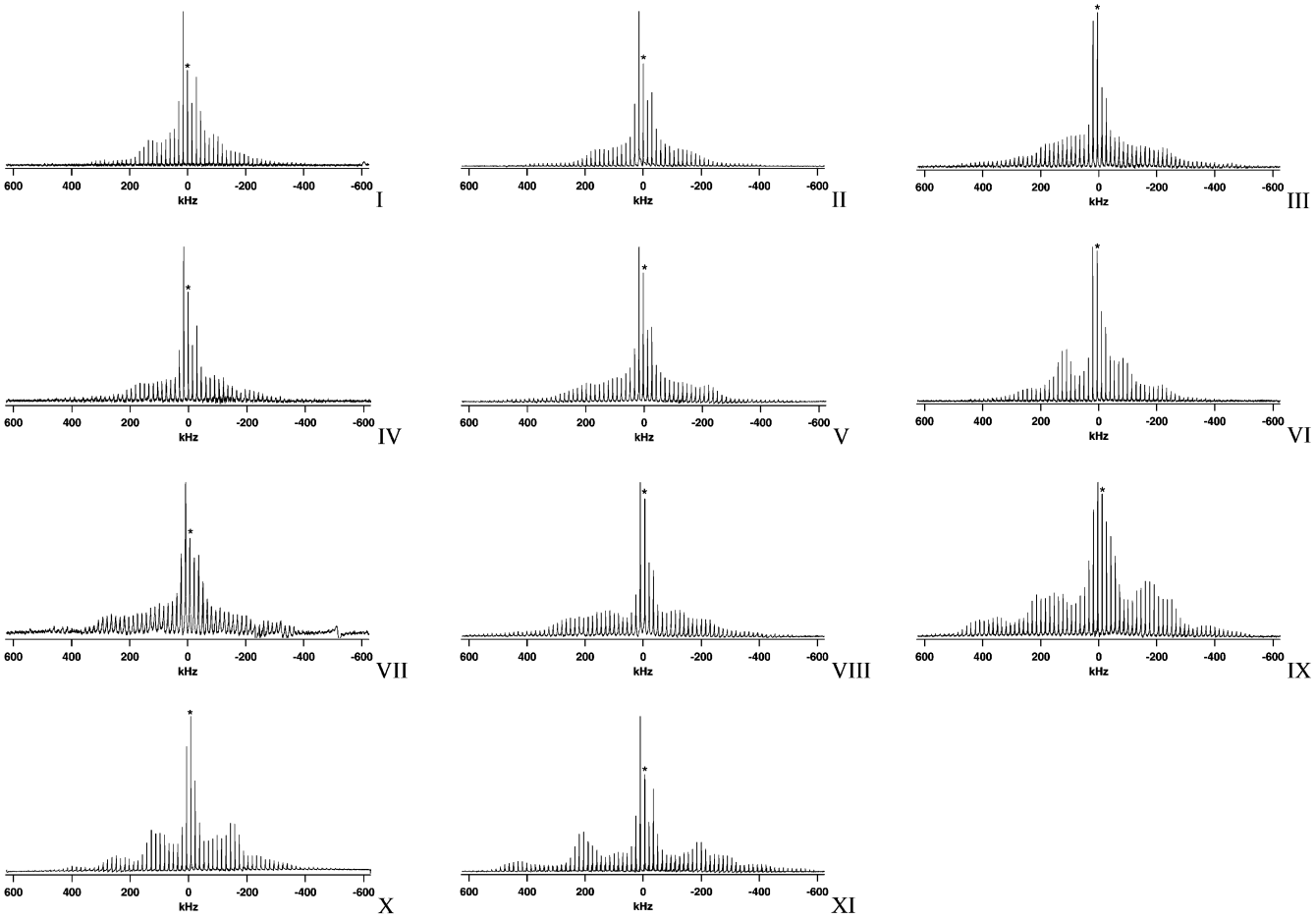

Figure 1. ^{51}V MAS NMR spectra of the oxovanadium(V) complexes acquired at 9.4 T and spinning speed 15 kHz. The anisotropic spinning sideband patterns appear to be very sensitive to the details of the molecular environment of the V center, as is manifested by the broad repertoire of the spectral lineshapes for the different compounds in this series. The numbering of the individual spectra corresponds to that of the complexes. The center bands are indicated by asterisks. The spectra are plotted on the same horizontal scale. The scale is in kilohertz to illustrate the variation in the overall widths of the anisotropic lineshapes, corresponding to variations in the quadrupolar coupling constants.

Table 3. Experimental Solid-State NMR Parameters for the Oxovanadium(V) Complexes: ^{51}V Isotropic Chemical Shifts (δ_{iso}), Quadrupolar Couplings (C_Q, η_Q), Chemical Shielding Anisotropies (δ_σ, η_σ), and the Euler Angles (α, β, γ) Describing the Relative Orientations of the Two Tensors

cmpd	C_Q, MHz	η_Q	δ_σ, ppm	η_σ	α, deg	β, deg	γ, deg	δ_{obsd}, ppm (solid state)	quadrupole induced shift, ppm	δ_{iso}, ppm (solid state)	δ_{iso}, ppm (solution)
I SJZ0040	3.07 ± 0.16	0.82 ± 0.13	496 ± 22	0.18 ± 0.17	0 ± 70	0 ± 15	0 ± 70	-453.9 ± 3	-2.2	-451.7 ± 3	-458
II SJZ0041	3.87 ± 0.3	0.77 ± 0.08	501 ± 29	0.07 ± 0.09	0 ± 30	0 ± 30	0 ± 30	-468.4 ± 0.5	-3.5	-464.9 ± 0.5	-466
III SJZ0032	3.90 ± 0.16	0.77 ± 0.16	380 ± 14	0.05 ± 0.05	0 ± 30	0 ± 15	0 ± 30	-419.7 ± 3	-3.5	-416.2 ± 3	-435
IV SJZ0069	4.00 ± 0.20	0.75 ± 0.10	504 ± 28	0.15 ± 0.28	0 ± 30	0 ± 15	0 ± 30	-451.9 ± 1.5 -459.2 ± 1.5	-3.7	-448.2 ± 1.5	-450
V JZ0060	5.10 ± 0.34	0.60 ± 0.10	466 ± 28	0.10 ± 0.24	0 ± 30	0 ± 15	0 ± 30	-434.6 ± 2	-6.0	-428.6 ± 2	-435
VI SJZ0068	3.65 ± 0.1	0.22 ± 0.07	375 ± 19	0.008 ± 0.10	0 ± 30	0 ± 15	0 ± 30	-407.8 ± 1.5	-3.1	-404.7 ± 1.5	-436
VII SJZ00108	6.00 ± 0.40	0.70 ± 0.05	570 ± 19	0.6 ± 0.10	0 ± 60	0 ± 10	30 ± 30	$+417 \pm 3$	-9.3	$+426.3 \pm 3$	$+422, +375$
VIII HS001	5.67 ± 0.25	0.45 ± 0.05	433 ± 28	0.30 ± 0.15	0 ± 30	0 ± 15	0 ± 30	-517.5 ± 2	-7.6	-510 ± 2	$-523, -534$
IX HS003	6.23 ± 0.19	0.2 ± 0.05	728 ± 29	0.7 ± 0.10	25 ± 18	48 ± 11	57 ± 10	-575.2 ± 3	-10.4	-564.8 ± 3	-607
X Sal50Et	4.35 ± 0.19	0.00 ± 0.05	336 ± 68	0.35 ± 0.10	0 ± 15	83 ± 16	80 ± 20	-372.0 ± 1 -375.0 ± 1	-4.5	-368.0 ± 1 -371.0 ± 1	-399
XI VO_2(acpy-inh)	7.00 ± 0.1	0.25 ± 0.05	485 ± 29	0.20 ± 0.1	70 ± 20	75 ± 15	0 ± 10	-515.5 ± 2	-11.4	-504.1 ± 2	-507

values and, therefore, have to be taken into account. For the compounds reported in this work, these upfield shifts ranged from -2.2 to -11.4 ppm.

In agreement with solution NMR results, most of the complexes are strongly shielded, exhibiting isotropic shifts in the range ca. -400 to -600 ppm. **VII** is the only exception ($\delta_{iso} = +417 \pm 3.6$ ppm) due to the "noninnocent" bis(*tert*-butyl)-catecholate ligand, as discussed. The V(V) compounds with bis(*tert*-butyl)-catecholate ligands often contain admixtures of the V(IV) catecholate complex.[1] Our experimental solid-state NMR results indicate broadening of the individual lines in **VII**, which is consistent with the presence of the paramagnetic V(IV) centers. The comparatively low shielding in **X** ($\delta_{iso} = -368$ and -371 ppm) reflects the presence of a "soft" sulfur function in direct coordination to vanadium.

For **III**, **VI**, **VIII**, **IX**, and **X**, large discrepancies have been observed (ca. 15−30 ppm) between isotropic chemical shifts in solution and in the solid state, which cannot be explained by the quadrupolar induced shift. We attributed these variations to the high sensitivity of the chemical

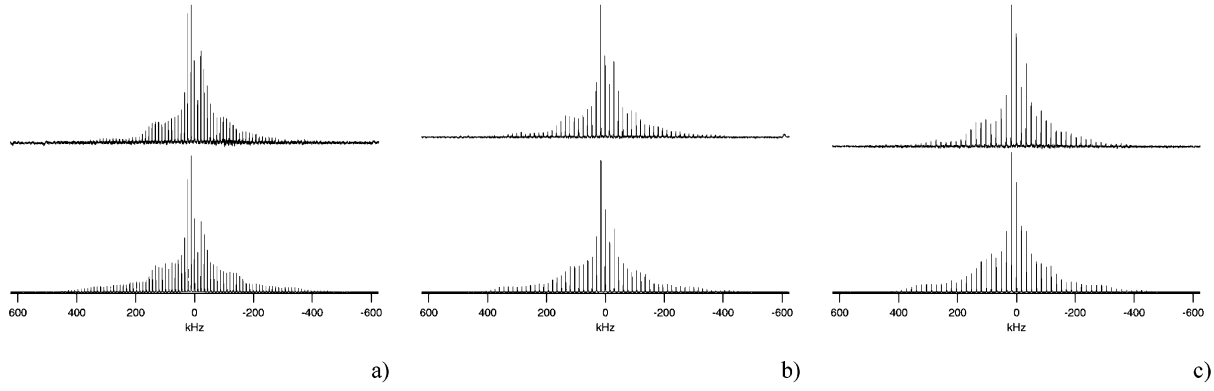

Figure 2. Experimental (top) and simulated (bottom) ^{51}V MAS NMR spectra of **I** (SJZ0040) at (a) 11.0, (b) 15.0, and (c) 17.0 kHz. The spectra were simulated using the following parameters: $C_Q = 3.07$ MHz; $\delta_\sigma = 496$ ppm; $\eta_Q = 0.82$; $\eta_\sigma = 0.18$; $\alpha = 0°$; $\beta = 0°$; $\gamma = 0°$. The rmsd values were (a) 0.11, (b) 0.11, (c) 0.12.

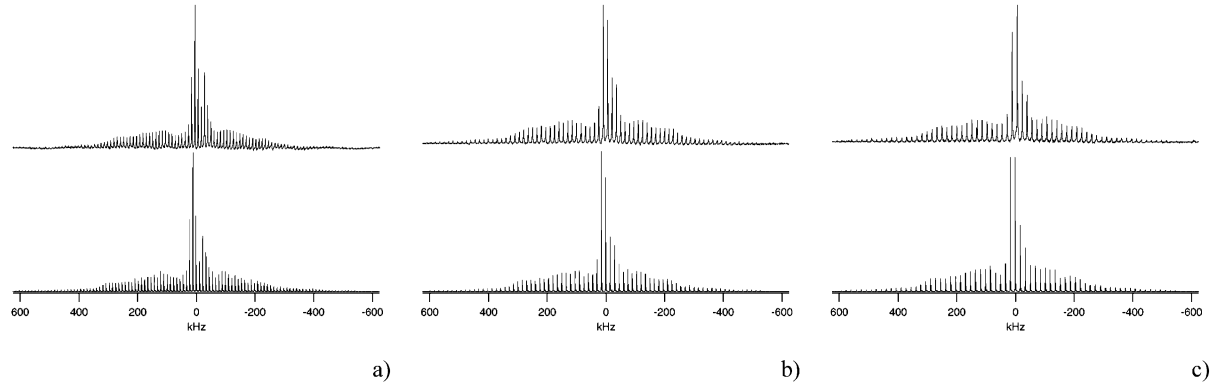

Figure 3. Experimental (top) and simulated (bottom) ^{51}V MAS NMR spectra of **VIII** (HS001) at (a) 11.0, (b) 15.0, and (c) 17.0 kHz. The spectra were simulated using the following parameters: $C_Q = 5.67$ MHz; $\delta_\sigma = 433$ ppm; $\eta_Q = 0.45$; $\eta_\sigma = 0.30$; $\alpha = 0°$; $\beta = 0°$; $\gamma = 0°$. The rmsd values were (a) 0.06, (b) 0.08, (c) 0.06.

shielding interaction at the vanadium nucleus to the changes in local environment. It is likely that solvent molecules of DMSO and THF interact with the central vanadium atom in solution, causing the expansion of the coordination sphere. The solid-state isotropic chemical shifts for the remaining compounds were in good agreement with solution NMR data.

Numerical Simulations of the ^{51}V Solid-State NMR Spectra. The parameters describing the quadrupolar and CSA interactions were determined from numerical simulations of the solid-state NMR spectra and are reported in Table 3 for each of the compounds. The asymmetry of the lineshapes in the MAS spectra is a result of the combined effect of the anisotropic quadrupolar and CSA interactions. The anisotropic spectral envelope is described by seven independent parameters: the anisotropy and the asymmetry of the quadrupolar and CSA tensors (C_Q, η_Q, δ_σ, and η_σ), and the three Euler angles (α, β, and γ) relating the principal axes system of the quadrupolar and CSA tensors. For ^{51}V and a number of half-integer quadrupolar nuclei, the quadrupolar and CSA interactions are orders of magnitude different in strength, thus allowing determination of the seven independent parameters describing these interactions from a single MAS spectrum.

We acquired and simulated MAS spectra for each of the compounds at three different spinning speeds, in order to be able to extract with greater accuracy the quadrupolar and CSA tensor elements, and to obtain reliable error estimates. This was particularly important because there have been no reports in the literature concerning ^{51}V solid-state NMR for similar classes of compounds, and the possible magnitudes of the quadrupolar and CSA interactions have been not known. Moreover, seven of the oxovanadium complexes under investigation are amorphous powders and resisted our attempts for crystallization and crystallographic characterization, preventing us from estimating the anisotropic interactions from point monopole calculations based on the local geometry of the vanadium atom.

In Figures 2 and 3, representative experimental and simulated spectra are shown for **I** and **VIII**. Spectra for the remaining compounds are presented in the Supporting Information (Figures 1s−9s). The numerical calculations for NMR spectra at three different spinning speeds demonstrate good convergence for all compounds, attesting to the high precision of both the measurements and the simulations.

According to the experimental and simulated results, the magnitude of the quadrupolar coupling constant, C_Q, varies from ca. 3.06 to ca. 7 MHz for the complexes under investigation. These variations are caused both by the nature of the coordination environment and by the differences in geometry. For example, the largest C_Q values were observed for **IX** and **XI**, whose geometry and electronic environment of the first coordination sphere appear to result in the most asymmetric charge distribution on the central vanadium atom. **VII** contains a "noninnocent" catecholate ligand and also

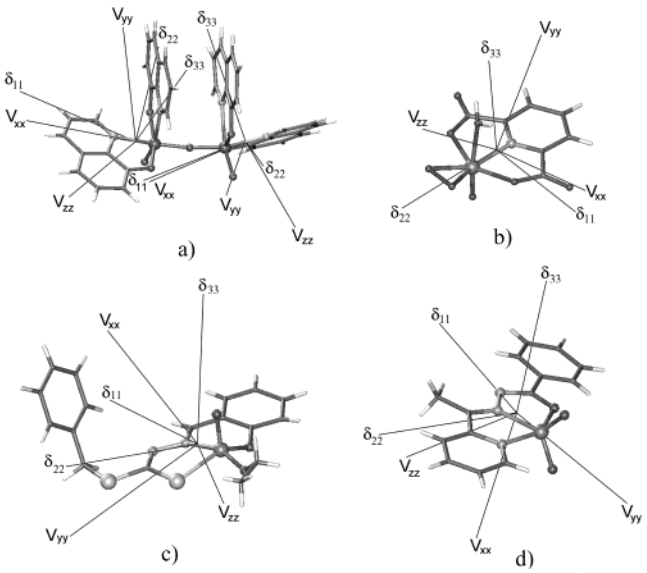

Figure 4. Molecular structures of compounds (a) **VIII**, (b) **IX**, (c) **X**, (d) **XI**. The orientations of the chemical shielding anisotropy and electric field gradient tensors with respect to the molecule fixed frame were calculated at the b3lyp/TZV level and are displayed for each compound. The principal components of the CSA tensor are designated as (δ_{11}, δ_{22}, δ_{33}), and those of the EFG tensor as (V_{xx}, V_{yy}, V_{zz}). The central vanadium atoms are depicted as spheres of the largest diameter and are colored dark gray, carbon and hydrogen atoms are shown as sticks of dark and light gray color, respectively, nitrogens are shown as light spheres of intermediate size, and oxygens are darker spheres of intermediate size. Sulfur atoms are shown as large light gray spheres.

displays a large quadrupolar anisotropy. In compounds **I**−**VII**, the quadrupolar and CSA tensors appear to be coincident. The CSA tensors are very close to axial, while the quadrupolar tensors exhibit significant rhombicity.

The nature of the first coordination sphere atoms and the geometry of **I**−**VII** is similar, as already discussed, and we expected little variation in the quadrupolar and CSA anisotropies in these complexes. However, pronounced differences in both parameters are observed experimentally (Table 3): C_Q ranges from 3.06 to 5.9 MHz, and δ_σ ranges from 376 to 561 ppm. We attribute these variations to the distinct electronic structure of the individual ligands. The low δ_σ values go along with compounds having a hydroxamato coligand (**III** and **VI**). Low shielding in hydroxamato complexes has been noted previously.[72] Electrostatic calculations of the EFG tensor based on point charges would be meaningless for these molecules because of the complex electronic structure of the ligands. Quantum mechanical calculations could potentially provide a clearer answer. In the absence of crystal structures for **I**−**VII**, these calculations are computationally expensive and will be attempted in a separate study.

Electrostatic and DFT Calculations of EFG Tensors and Nuclear Magnetic Shieldings for VIII−**XI.** These four compounds have been crystallographically characterized.[48−50,73] Their 3D structures are shown in Figure 4.

We have attempted to use the electrostatic model to calculate the EFG tensor on the vanadium atom based on the X-ray coordinates and the partial charges, computed using the bond-valence approach as described in the Materials and Methods subsection. For all four compounds **VIII**−**XI**, the electrostatic model appears to systematically underestimate C_Q (Table 4). The asymmetry parameters are also in disagreement with the experimental results. Thus, this simple model, which has been demonstrated to work quite well in ionic systems,[22−24,39] fails for the compounds with significant covalent bond character, such as the oxovanadium(V) complexes described here. That the covalent compounds would not be adequately described using the electrostatic model was anticipated by Koller et al.[39]

On the other hand, the DFT calculations yield very reasonable agreement with the experimental solid-state NMR data for both TZV and 6-311+G basis sets (Table 4). Both the anisotropy and asymmetry values of the quadrupolar tensor could be reproduced by the DFT calculations. Interestingly, the DFT theoretical results predict low rhombicity for the quadrupolar tensor, in agreement with the solid-state NMR data, and contrary to predictions based on the electrostatic model. For **XI**, the DFT calculations using both basis sets yield a negative sign for C_Q. The signs of the quadrupolar coupling constant cannot be inferred from solid-state NMR data, and theoretical calculations thus complement nicely the experiment.

The calculated chemical shielding anisotropies with DFT/B3LYP are in reasonable agreement with the experimental data for **VIII**, **IX**, and **XI** (Table 4). For **VIII**, the experimental solid-state NMR spectra indicate two magnetically equivalent vanadium atoms, as confirmed by the calculation. For **X**, there is a large discrepancy between experiment and calculations. We attribute this to the presence of a sulfur atom coordinated to vanadium, and it is likely that TZV and 6-311+G basis sets do not provide an adequate description of the system.

The orientations of the CSA and EFG tensors in the molecular reference frame were inferred from the DFT calculations. The results are summarized in Figure 4 and Table 4. According to the calculations, the most shielded δ_{33} component of the CSA tensor in **VIII**−**XI** is almost perpendicular to the plane formed by the heterocycles, with the other two components approximately lying in this plane. The orientation of the EFG tensor differs among **IX**−**XI**. In **VIII**, the largest V_{zz} component is almost parallel to δ_{33} with $\beta = 10.0°$; in **IX**, V_{zz} forms an angle of 44.4° with the plane formed by the heterocycles, while in **X** and **XI**, V_{zz} is located in this plane and almost perpendicular to δ_{33}. Thus, the CSA and EFG tensors are noncoincident, confirming the experimental solid-state NMR conclusions. The final Euler angles describing the mutual orientations of the tensors are summarized in Table 4. The results indicate excellent agreement between experimental and computed polar angle β. The azimuthal angles α and γ show larger deviations between the computed and experimental values, which is expected due to the low degree of rhombicity in either quadrupolar (in **IX**), or CSA (in **VIII**), or both tensors (in **X** and **XI**). Overall, the agreement between theory and experiment is

(72) Smith, P. D.; Berry, R. E.; Harben, S. M.; Beddoes, R. L.; Helliwell, M.; Collison, D.; Garner, C. D. *J. Chem. Soc., Dalton Trans.* **1997**, *23*, 4509−4516.
(73) Mauraya, M. R.; Khurana, S.; Schulzke, C.; Rehder, D. *Eur. J. Inorg. Chem.* **2001**, *3*, 779−788.

Table 4. Quadrupolar Interaction and Chemical Shielding Anisotropy Parameters for the Crystallographically Characterized Compounds **VIII**−**XI** Calculated from the Electrostatic Model and DFT Calculations Using B3LYP Exchange-Correlation Functional (*Gaussian98*) in Comparison with Solid-State NMR Experimental Results

cmpd	method	C_Q (MHz)	η_Q	δ_σ (ppm)	δ_{iso} (ppm)	η_σ	α (deg)	β (deg)	γ (deg)
VIII HS001	expt	5.67 ± 0.25	0.45 ± 0.05	433 ± 28	−510 ± 2	0.30 ± 0.15	0 ± 30	0 ± 15	0 ± 30
	b3lyp/TZV	6.87/6.87	0.44/0.44	496.0/496.3	−835.1	0.13/0.13	25.2/25.2	10.0/10.0	46.2/46.1
	b3lyp/6-311+G	8.03/8.03	0.33/0.34	485.5/485.8	−791.8	0.12/0.12	27.4/26.6	10.7/10.6	47.4/47.4
	electrostatic model	3.7	0.9						
IX HS003	expt	6.23 ± 0.19	0.2 ± 0.05	728 ± 29	−564.8 ± 2	0.70 ± 0.10	25 ± 18	48 ± 11	57 ± 30
	b3lyp/TZV	5.14	0.28	718.4	−779.2	0.56	89.5	45.6	78.5
	b3lyp/6-311+G	6.23	0.24	722.9	−756.6	0.56	89.8	46.3	78.1
	electrostatic model	5.7	0.27						
X Sal50Et	experiment	4.35 ± 0.19	0.00 ± 0.05	336 ± 68	−368.0 ± 1/ −371.0 ± 1	0.35 ± 0.10	0 ± 15	83 ± 16	80 ± 20
	b3lyp/TZV	4.05	0.03	468.7	−1016.8	0.24	23.9	86	52
	b3lyp/6-311+G	4.44	0.154	458.1	−554.7	0.25	25.8	86.1	74.6
	electrostatic model	3.71	0.75						
XI VO_2(acpy-inh)	expt	7.00 ± 0.05	0.25 ± 0.05	485 ± 29	−504.1 ± 2	0.25 ± 0.05	70 ± 20	75 ± 15	0 ± 10
	b3lyp/TZV	−8.45	0.29	551.9	−791.1	0.10	73.7	89.2	4.7
	b3lyp/6-311+G	−9.52	0.35	546.0	−746.0	0.07	68.4	89.3	3.5
	electrostatic model	5.7	0.9						

very good, and both basis sets utilized in the calculations yield very similar orientations for the EFG and CSA tensors.

The isotropic chemical shifts display poor agreement with the experimental results, with the TZV basis set yielding a worse correlation with the experiment as compared with the 6-311+G basis set. It is somewhat surprising that the level of theory used in this work provides an adequate description of the anisotropic observables in the first place, given that the tensors were calculated for single molecules in a gas phase with no intermolecular interactions taken into account, and given the relatively small size of the basis sets used in the calculations. At present, we do not understand the source of the discrepancies between experimental and calculated chemical shifts. One possibility is that larger basis sets are necessary for the systems under investigation. Another possibility is that relativistic treatment needs to be employed, as was recently demonstrated by Bryce and Wasylishen for ^{95}Mo complexes.[44]

We point out that neither the experimental solid-state NMR spectroscopy alone nor the quantum mechanical calculations at the current level of theory have the ability to yield a complete and accurate description of the geometric and electronic parameters of the vanadium-containing systems. A combination of these two methods, however, appears to be very promising for analysis of diamagnetic oxovanadium molecules.

Conclusions

We have demonstrated that ^{51}V magic angle spinning solid-state NMR spectroscopy is a sensitive probe of the local geometry and electrostatic environment in a series of 11 novel oxovanadium(V) complexes modeling active site features of vanadium haloperoxidases. Electric field gradient and chemical-shielding anisotropy tensors are readily obtained from the spectra and bear a wealth of information about the local environment of the vanadium atoms in these complexes, information which is of potential importance for understanding differences in activities due to subtle variations in the active centers of vanadate-dependent haloperoxidases from different microorganisms. Both proximal and distal ligands significantly affect the electrostatic environment at the vanadium site, resulting in different fine structure constants for compounds with chemically and geometrically similar vanadium first coordination spheres. A combination of experimental solid-state NMR spectroscopy and theoretical hybrid DFT calculations can provide an accurate description of the molecular and electronic structure in the vanadium-containing systems, as has been shown for the four crystallographically characterized complexes addressed in this work. This combination of methods can become particularly useful for investigation of difficult-to-crystallize molecules containing diamagnetic vanadium(V) sites.

Acknowledgment. We thank Professor Ann McDermott of Columbia University (New York, NY) for NMR spectrometer time at 7.1 T for the preliminary measurements. T.P. thanks Dr. Arno Kentgens (University of Nijmegen, The Netherlands) for very helpful discussions on the electrostatic calculations of the EFG tensors and for the Turbo-Pascal PC program for these calculations. We thank Prof. Niels C. Nielsen and co-workers for the SIMPSON program. T.P. acknowledges financial support of Hunter College, support from PSC-CUNY, and support from AFOSR/NI HBCU/MI instrumentation program (Grant F49620-00-1-0352). The project was in part supported by the Deutsche Forschungsgemeinschaft (Grant RE 431/13-3).

Note Added after ASAP: In the version of this paper posted ASAP on January 25, 2003, a 2 exponent in eq 6 was mistakenly not a superscript. In addition, due to a production error, the column heads of Tables 3 and 4 contained η_s instead of η_σ. These characters are correct in the version posted on January 29, 2003.

Supporting Information Available: Additional figures. This material is available free of charge via the Internet at http://pubs.acs.org.

IC026141E